Cardiovasc Intervent Radiol (2013) 36:1638–1645
DOI 10.1007/s00270-013-0704-1

CIRSE

LABORATORY INVESTIGATION

The Effects of Metallic Implants on Electroporation Therapies: Feasibility of Irreversible Electroporation for Brachytherapy Salvage

Robert E. Neal II · Ryan L. Smith · Helen Kavnoudias · Franklin Rosenfeldt · Ruchong Ou · Catriona A. Mclean · Rafael V. Davalos · Kenneth R. Thomson

Received: 12 February 2013 / Accepted: 3 July 2013 / Published online: 14 August 2013

Abstract
Purpose Electroporation-based therapies deliver brief electric pulses into a targeted volume to destabilize cellular membranes. Nonthermal irreversible electroporation (IRE) provides focal ablation with effects dependent on the electric field distribution, which changes in heterogeneous environments. It should be determined if highly conductive metallic implants in targeted regions, such as radiotherapy brachytherapy seeds in prostate tissue, will alter treatment outcomes. Theoretical and experimental models determine the impact of prostate brachytherapy seeds on IRE treatments.
Materials and Methods This study delivered IRE pulses in nonanimal, as well as in ex vivo and in vivo tissue, with and in the absence of expired radiotherapy seeds. Electrical current was measured and lesion dimensions were examined macroscopically and with magnetic resonance imaging. Finite-element treatment simulations predicted the effects of brachytherapy seeds in the targeted region on electrical current, electric field, and temperature distributions.
Results There was no significant difference in electrical behavior in tissue containing a grid of expired radiotherapy seeds relative to those without seeds for nonanimal, ex vivo, and in vivo experiments (all $p > 0.1$). Numerical simulations predict no significant alteration of electric field or thermal effects (all $p > 0.1$). Histology showed cellular necrosis in the region near the electrodes and seeds within the ablation region; however, there were no seeds beyond the ablation margins.
Conclusion This study suggests that electroporation therapies can be implemented in regions containing small metallic implants without significant changes to electrical and thermal effects relative to use in tissue without the

R. E. Neal II (✉) · H. Kavnoudias · K. R. Thomson
Radiology Research Unit, Department of Radiology, The Alfred Hospital, 1st Floor Philip Block, 55 Commercial Road, Melbourne, VIC 3004, Australia
e-mail: robert.neal@alfred.org.au

H. Kavnoudias
e-mail: H.Kavnoudias@alfred.org.au

K. R. Thomson
e-mail: K.Thomson@alfred.org.au

R. L. Smith
William Buckland Radiotherapy Centre, The Alfred Hospital, 55 Commercial Road, Melbourne, VIC 3004, Australia
e-mail: ryan.smith@wbrc.org.au

F. Rosenfeldt · R. Ou
Department of Surgery, Monash University, 55 Commercial Road, Melbourne, VIC 3004, Australia
e-mail: F.Rosenfeldt@alfred.org.au

R. Ou
e-mail: Ruchong.Ou@bakeridi.edu.au

C. A. Mclean
Department of Anatomical Pathology, The Alfred Hospital, 55 Commercial Road, Melbourne, VIC 3004, Australia
e-mail: C.Mclean@alfred.org.au

R. V. Davalos
School of Biomedical Engineering and Sciences, Virginia Tech, 329 ICTAS Building, Stranger St. (MC 0298), Blacksburg, VA 24061, USA
e-mail: davalos@vt.edu

implants. This supports the ability to use IRE as a salvage therapy option for brachytherapy.

Keywords IRE · Non-thermal focal ablation · Translational oncology models · Heterogeneous tissue · Minimally invasive surgery · Cancer therapy

Introduction

Electroporation-based therapies (EBTs) use small needle electrodes placed into or around targeted tissue to deliver a series of intense (1–3 kV), however, brief (~50–100 μs) electric pulses that alter native cellular transmembrane potentials, thus creating nanoscale defects in cellular membranes. In reversible electroporation, defect creation with cell survival facilitates macromolecule transport, including chemotherapeutics and genetic material [18, 24]. With appropriate electric pulse parameters, the defects are irrecoverable, and the cells die in a nonthermal manner known as irreversible electroporation (IRE).

IRE provides minimally invasive tumor ablation [6], reaching up to 92 % tumor control in cutaneous and orthotopic models [1, 23]. Canine clinical cases demonstrate IRE's ability to treat complex unresectable tumors, including a large sarcoma and a glioma [11, 22]. A phase I human safety study attained complete target tumor ablation in 46 of 69 tumors unresponsive to or ineligible for other therapies [29] with treatments well-tolerated by patients [3, 19].

IRE exhibits submillimeter demarcation between treated and unaffected cells [7]. Tissue property changes enable real-time treatment monitoring [2, 28]. The lethal zone relates to the electric field distribution, thus permitting treatment planning by way of numerical modeling [17]. IRE is unaffected by blood perfusion "heat-sink" and appears to spare sensitive structures, such as major vasculature and ductal systems [7, 25], thus enabling treatment of tumors unresectable and ineligible for thermal ablation.

Prostate cancer is the most common cancer in men [4]. Radiation therapy, including brachytherapy by way of iodine-125 seed implantation, is a common treatment. Although often able to attain local tumor control, an estimated 10 % of low-risk and 60 % of high-risk patients develop biochemical relapse [4, 26]. When relapse is due to local-only tumor recurrence, patients may benefit from local salvage treatments, including radical prostatectomy, cryotherapy, salvage brachytherapy, and high-intensity focused ultrasound. These techniques carry varying complication risks, including urinary incontinence, rectal injury, and erectile dysfunction, and efforts to mitigate these risks may decrease effectiveness to the sensitive regions [8, 16]. IRE's advantages as a nonthermal therapy make it a promising salvage treatment option.

Heterogeneous tissue conductivity distributions can modify IRE treatment outcomes by altering electric field distribution and thermal effects [17, 20]. If IRE is to be used in proximity of metallic implants, such as brachytherapy seeds, changes to the electrophysical behavior of the electric pulses from these highly conductive materials must be understood. This study uses multiple theoretical and experimental models to determine the relative impact of brachytherapy seed metallic implants on IRE treatment effects in healthy prostate tissue.

Methods

Experiments Using Non-mammalian Tissue

Potato tuber cells exhibit dynamic conductivity electroporation responses similar to in vivo animal tissue [14]. Electroporation-induced intracellular content release locally alters affected tissue properties, thus allowing visualization of electroporated regions [13]. These features permit the use of potato tuber as a low-cost preliminary tool to examine IRE effects, including electrical current and lesion dimensions. Potato tuber samples (~8 cm diameter) were secured inside a radiotherapy seed guidance system. Three placement needles, each containing three brachytherapy seeds, were used to insert a total of nine seeds, with two electrodes inserted perpendicular to the seed axis (Fig. 1A). The seeds were in the region exposed to the highest electric field, where effects would be most pronounced.

An ECM830 generator (Harvard Apparatus, Cambridge, MA, USA) (Fig. 1B) delivered 10 square wave electric pulses, each 100 μs long, at a rate of one pulse per second with a strength of 1,750 V (1,750 V/cm voltage-to-distance ratio), which is similar to clinical IRE therapies. Electrical current was measured with a Tektronix TCP305 electromagnetic induction current probe placed around the wire of the grounded electrode and connected to a TCPA300 amplifier (both from Tektronix, Beaverton, OR, USA). This probe measures the electrical current-induced magnetic field around a wire to determine the electrical current flowing through it. A Protek DS0-2090 USB computer-interface oscilloscope provided current measurements on a laptop using the included DSO-2090 software (both from GS Instruments, Incheon, Korea) (Fig. 1B). Electrical currents from the potatoes with and without seeds were measured and analyzed at pulses 1, 5, and 10 to determine the average current for both groups ($n \geq 8$). Magnetic resonance imaging (MRI) performed 16–24 h after pulse delivery used a GE 1.5T scanner with T1, T2, and T1 three-dimensional spin gradient sequences, all with 3 mm slice

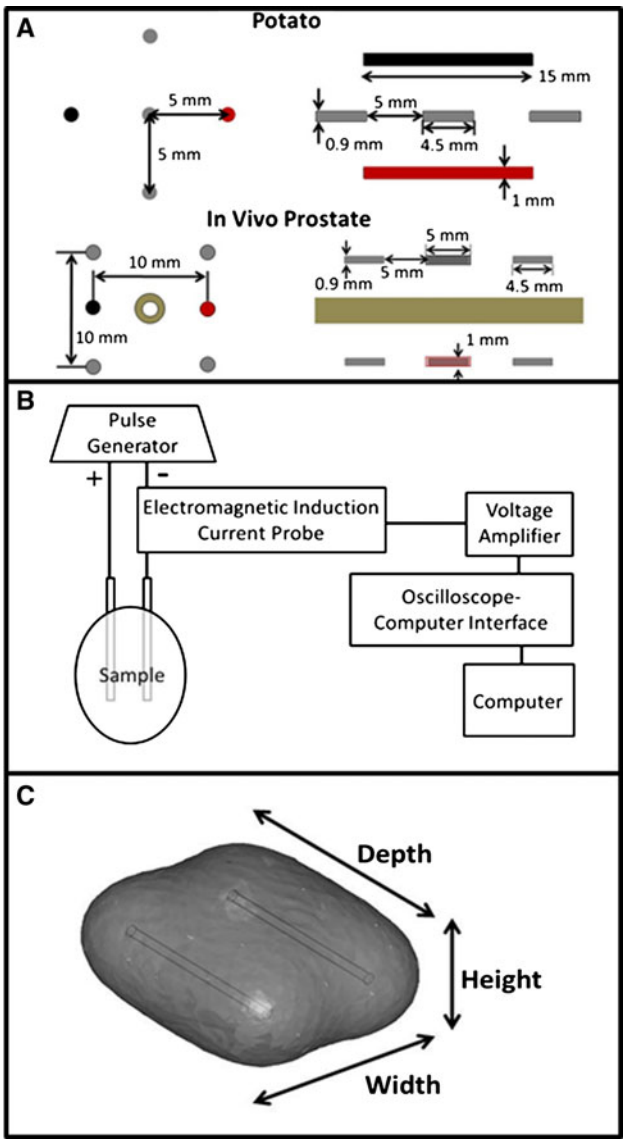

Fig. 1 Experimental setup. **A** Potato and in vivo prostate experimental geometry for radiotherapy seeds (*gray*), cathode (*black*), and anode (*red*) with relevance to urethra (*tan*). **B** Schematic of electrical pulse measuring system. **C** Orientation for lesion height, width, and depth measurements

thickness. Images were analyzed to determine the maximum lesion width, height, and depth (Fig. 1C).

Animal Experiments

In addition to the tuber experiments, ablations were performed on canine prostates, two in vivo in an Animal Ethics—approved procedure and two ex vivo from animals in an unrelated study. In each case, one prostate was pulsed without seeds and the effects were compared with a prostate with 12 (in vivo) or 18 (ex vivo) seeds. The in vivo trials were performed with both canines under intravenous general anesthesia via propofol induction (6 mg/kg and then 0.5 mg/kg/min) and maintained by inhaled isofluorane (1–2 %) as confirmed by a bispectral index monitor (Covidien, Dublin, Ireland) with intravenous pancuronium muscle blockade (0.1–0.3 mg/kg) to eliminate muscle contraction; the dosage was adjusted based on the extent of visible muscle contraction. Electrodes were inserted along the direction of the urethra, with one in each the left and right hemispheres (Fig. 1A), with 1.0 cm (in vivo) and 1.5 cm (ex vivo) separations.

After electrode placement, a single prepulse of 50 V/cm voltage-to-distance ratio was delivered to determine baseline conductivity. After the prepulse, a total of 100 pulses, each 100 μs long at 1,250 V (1,250 V/cm) (in vivo) and 2,625 V (1,750 V/cm) (ex vivo), were delivered at a rate of one pulse per second. In vivo subjects were maintained for ~4.5 h under anesthesia to permit adequate lesion development before euthanasia [2]. Prostates were then removed, formalin fixed, paraffin-embedded, and sectioned for staining with haematoxylin and eosin (H&E).

Numerical Simulations

Numerical models provide a flexible platform to rapidly investigate treatment effects under different experimental conditions [12, 17]. Here, they predict the electrical current, electric field, and temperature distributions in simulated IRE procedures in prostate tissue with varying numbers of brachytherapy seeds to determine what impact the metallic seeds may have on treatment outcomes. This was performed using the finite modeling software Comsol Multiphysics v3.5a (Comsol, Stockholm, Sweden) to simulate a 10 cm diameter spherical tissue domain with two 1 mm diameter electrodes in the center (properties Table 1), each 1.5 cm long and separated by 1 cm, with a single 1,750 V, 100 μs long pulse applied between them.

Statistical Analysis

Statistical significance was computed with analysis of means and one-way analysis of variance (ANOVA) to compare conditions with seeds relative to ones that did not using JMP 9 (SAS, Cary, NC, USA). Numerical model integrated volumes with seeds are presented as a percentage of difference from the no-seed conditions.

Results

Current Data

Currents were analyzed at pulses 1, 5, and 10 from the potato tubers during the pulse ($n = 9$, Fig. 2), and ANOVA comparing the averaged final 80 to 100 μs portion of the

Table 1 Tissue thermal and electrical properties for numerically modeled prostate tissue

Property	Symbol	Value
Heat capacity [J/(kg K)]	c_p	3600 [27]
Thermal conductivity [W/(m K)]	k	0.5 [27]
Density (kg/m^3)	ρ	1000
Blood perfusion term [W/(m^3 K)]	$w_b \cdot c_b$	40,000 [27]
Baseline electrical conductivity (S/m)	σ_0	0.4113 [5, 9, 10, 21]
Maximum electrical conductivity (S/m)	σ_{max}	0.8712 [9, 10, 21]

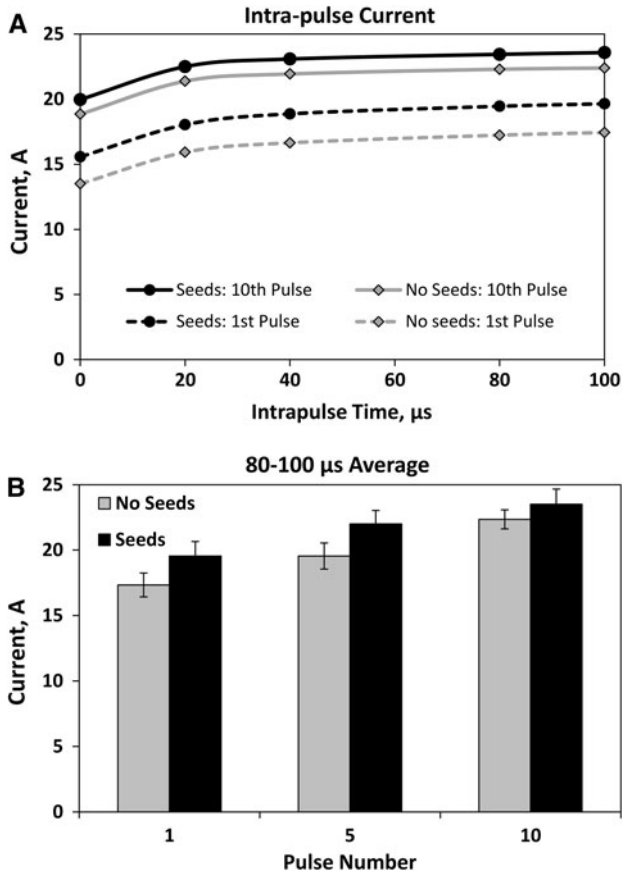

Fig. 2 Experimental potato currents. **A** Current at various intrapulse time points for pulses 1 and 10 without (*gray*) and with expired radiotherapy seeds (*black*). **B** Averaged currents with SEM (*bars*) from the final 80 to 100 µs without (*gray*) and with (*black*) the metallic implants for pulses 1, 5, and 10

pulse found no significant difference between the potatoes with versus without seeds for pulses 1, 5, or 10 ($p = 0.152$, 0.114, and 0.432, respectively).

Ex vivo experiments were performed within 3 h after death. They showed no significant difference in electrical current relative to the prepulse, which normalizes tissue properties between the different subjects. Electrical conductance increase was 79–103 % in the prostate with seeds and 81–117 % for the prostate without seeds.

In vivo current measurements at pulses 5, 45, and 95 yielded absolute currents of 4.8 ± 0.42 A and 5.8 ± 0.82 A for the prostates without and with seeds, respectively. Relative to the prepulse, conductance increases of 190 ± 17 % and 210 ± 30 % were observed without and with seeds, respectively. Analysis of means and ANOVA showed no significant difference between the presence of seeds in the raw currents ($p = 0.13$) nor conductance increase ($p = 0.30$).

Ablation Volumes

Potato Tuber

MRI showed distinct zones of affected tissue, best observed from T1s, likely due to a redistribution of fluid and intracellular contents (Fig. 3). No lesion was found in the 50 V/cm pulse control, whereas ANOVA of potatoes with versus without metallic seeds for lesion width and height resulted in p values of 0.124 and 0.870, respectively (Table 2), thus showing that affected volumes were unaltered by seed presence.

In Vivo Prostates

The electric pulses produced two circular ablation zones at the region of electrode placement. There was no significant ANOVA difference in lesion dimensions (Table 2) between the prostates with versus without seeds, with $p = 0.13$, 0.46, and 0.43 for height, width, and area, respectively. Histology shows hemorrhage in both prostates at the location of seed and electrode insertions (Fig. 4). H&E staining of the regions surrounding the electrodes in both prostates showed a discrete region of cellular necrosis. Tissue adjacent to seeds that were within the realm of ablation had the same appearance as the ablated prostate tissue without any seeds. Despite some local glandular hemorrhage at the location of radiotherapy seed placement, the cells and glands adjacent to seeds outside the IRE ablation region remained intact, thus matching regions beyond the IRE region in the prostate without seeds. This evidence shows the seeds did not locally alter microscale treatment effects at the site of the radiotherapy seeds relative to the inherent tissue changes from the pulses alone.

Numerical Simulations

The three numerical model physical geometry setups with representative electric field and temperature increase distributions are depicted in Fig. 5. The interelectrode currents for the models (Table 3) show that the maximum

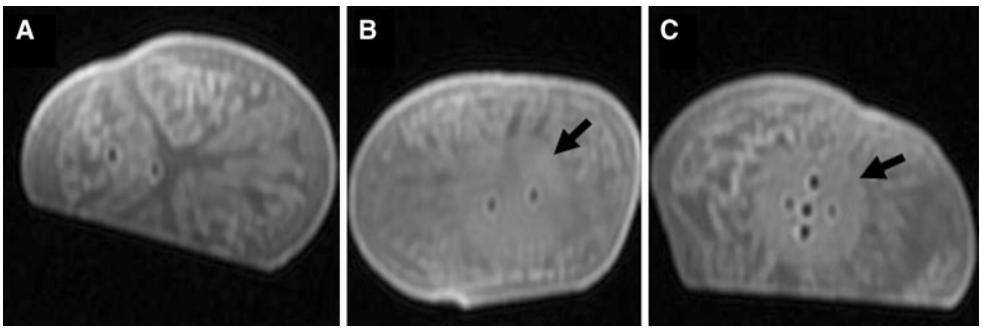

Fig. 3 Sample potato lesions. T1-weighted MRI images of potato trials **A** without pulses, **B** pulsed with electrodes only, and **C** pulsed in the presence of nine radiotherapy seeds. Regions exhibiting electroporation-induced changes can be seen (*arrows*)

Table 2 Electroporation-affected lesion dimensions

Model	Potato ($n \geq 8$)		Prostate ($n = 1$)	
	Electrodes only	Seeds	Electrodes only	Seeds
Width (cm)[a]	2.51 ± 0.05	2.41 ± 0.04	0.64 ± 0.03	0.73 ± 0.03
Height (cm)[a]	2.45 ± 0.08	2.43 ± 0.04	0.63 ± 0.02	0.66 ± 0.05
Area (cm^2)[a]	0.31 ± 0.02	0.35 ± 0.03	–	–

[a] Values are given as mean ± SE

difference was 14.7 % for the extrapolated grid relative to the model with no seeds. The integrated electric field and temperature volumes (Table 4) show no notable effect from the presence of seeds, where the average deviation for the models with seeds was 2.8 % relative to the simulation model without seeds.

Discussion

This investigation provides evidence from experimental and numerical models supporting the use of IRE near brachytherapy seeds or other small metallic implants without significantly altering electric pulse behavior or lesion dimensions. This is the first investigation into the impact of these heterogeneities on IRE protocols, which was explored with theoretical models and nonanimal tissue, as well as dead and living canine prostate tissue. Despite differences between potato and mammalian tissue, both showed that the inclusion of brachytherapy seeds had a negligible effect on tissue electrical characteristics and lesion dimensions. This builds on evidence supporting the use of potato tuber as a low-cost nonanimal analog for early investigation of electroporation effects under changing experimental conditions [14, 15, 21].

IRE has shown promising clinical results in various tumors. Its nonthermal modality is well-suited for treating prostate cancer because it has been shown to spare the urethra and neurovascular bundles often implicated in comorbidities of other prostate therapies [25]. However, current in vivo literature for prostate IRE remains limited to this canine study on healthy prostate, and future work should further characterize IRE in healthy, cancerous, and brachytherapy salvage prostate tissue.

Due to the absence of data regarding an IRE electric field threshold in prostate cancer, our model evaluated the effects from radiotherapy seed presence using electric fields relevant to previous in vitro and in vivo studies. The minimal change measured in exposed volume from the seeds should persist to other relevant electric fields. Furthermore, the relative changes to electric field distribution and thermal effects from the metallic implants will translate to other EBTs, suggesting that electrogenetransfer and electrochemotherapy should also be safe and relatively unaltered by metallic implants.

One difference between this investigation and true failed brachytherapy patients is the physical effects on the tissue properties from irradiation, which alters the cellular and stromal tissue aspects [4] and likely its electrical properties. Future work should examine the response of tumorous and previously irradiated tissue to determine reversible and lethal electric field thresholds to ensure that IRE's advantages are maintained. Previous evidence that describes sparing the extracellular matrix within ablated regions suggests that the electric pulses themselves should not pose significant risk to irradiated tissue beyond that from

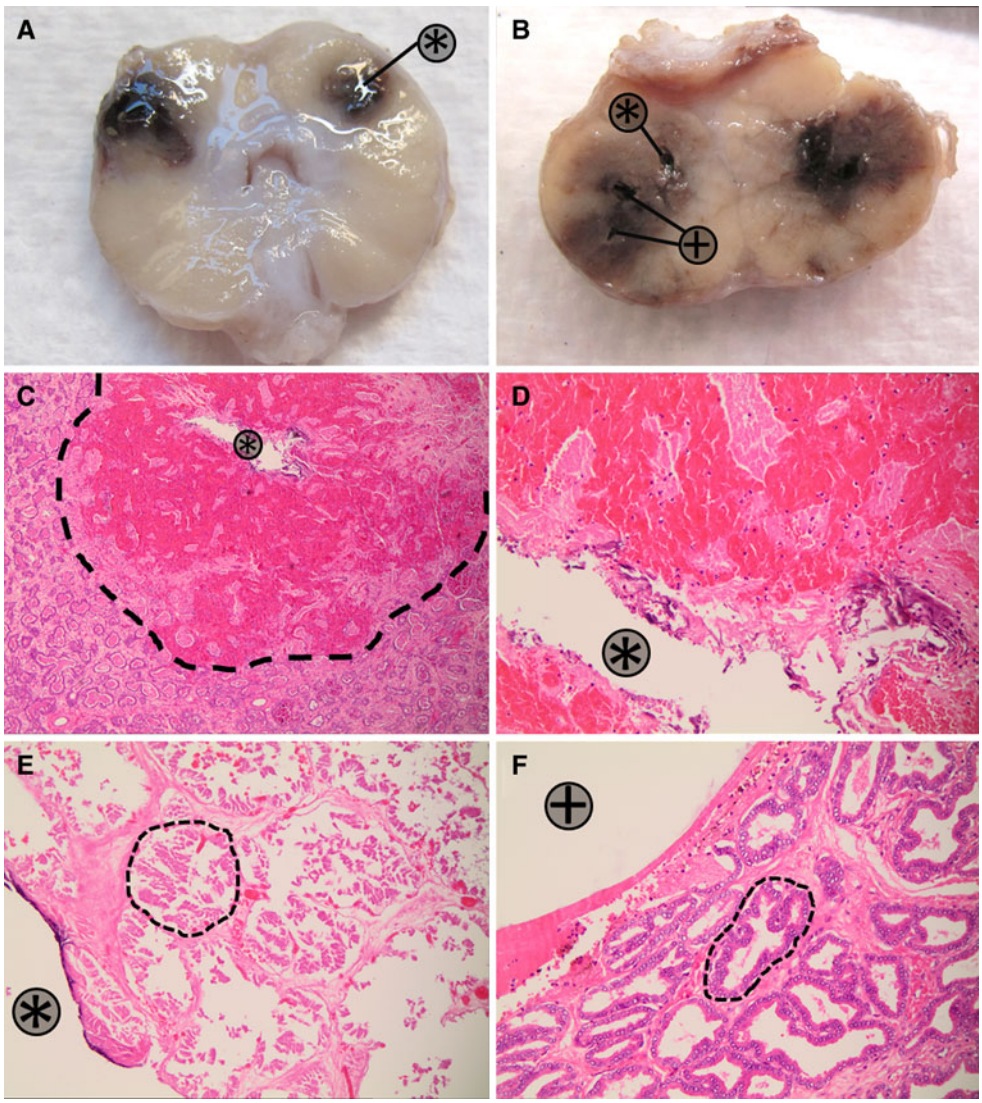

Fig. 4 In vivo prostate pathology. Macroscopic canine prostates after electroporation **A** without and **B** with radiotherapy seeds. Hemorrhage is evident at electrode and seed insertion points. (**C** [×40] and **D** [×200]) Electrode-insertion region (*asterisk*) in prostate without expired radiotherapy seeds shows hemorrhagic region with glandular necrosis (within *dashed* region). **E** Prostate with expired radiotherapy seeds shows complete cellular necrosis (necrotic gland denoted with *dashed* region) at electrode location (*asterisk*) within the ablation region, similar to ablated region within prostate tissue without expired radiotherapy seeds. (**F** [×200]) Expired radiotherapy seed location (*plus*) outside ablation region shows intact prostatic glands, which is consistent with glands beyond the ablation region in the prostate without any seeds (intact gland denoted within *dashed* region). All staining = H&E

physical electrode insertion, which is similar to salvage cryotherapy probes.

The thermal effects examined in the numerical model simulated a single pulse. Cumulative temperature increases in multiple pulse protocols may amplify the difference in thermal effects caused by the seeds, which can be mitigated with low total pulse numbers or pulse delivery rates.

Therapeutic IRE is locoregional in nature, thus making it applicable primarily for locally recurrent disease in brachytherapy salvage treatments. Despite the relatively small cohort of relapse patients eligible for IRE salvage, the low number of options and high morbidity rates from existing treatments in this group make it an important demographic to address where IRE's nonthermal mechanism has the potential to decrease some complications.

This study investigated the potential effect on EBTs, specifically IRE, induced by expired radiotherapy seeds as a model to mimic metallic implants with densely packed titanium pellets. The experimental and numerically modeled seed arrays represented typical packing density at the region where the greatest effects would be encountered. Greater densities or larger seeds will increase the proportional volume of metal relative to tissue, thus increasing the impact. However, this would likely remain insignificant for clinically relevant applications. Larger implants, such as vascular stents or pacemakers, may exert a more significant effect on treatment outcome. Although these should not contraindicate EBTs, consideration should be given to them to ensure that electric fields and currents remain within the targeted ranges and volumes to attain the desired treatment outcomes.

Conclusion

This study investigated the potential electrical and ablation dimension effects that would occur from using irreversible

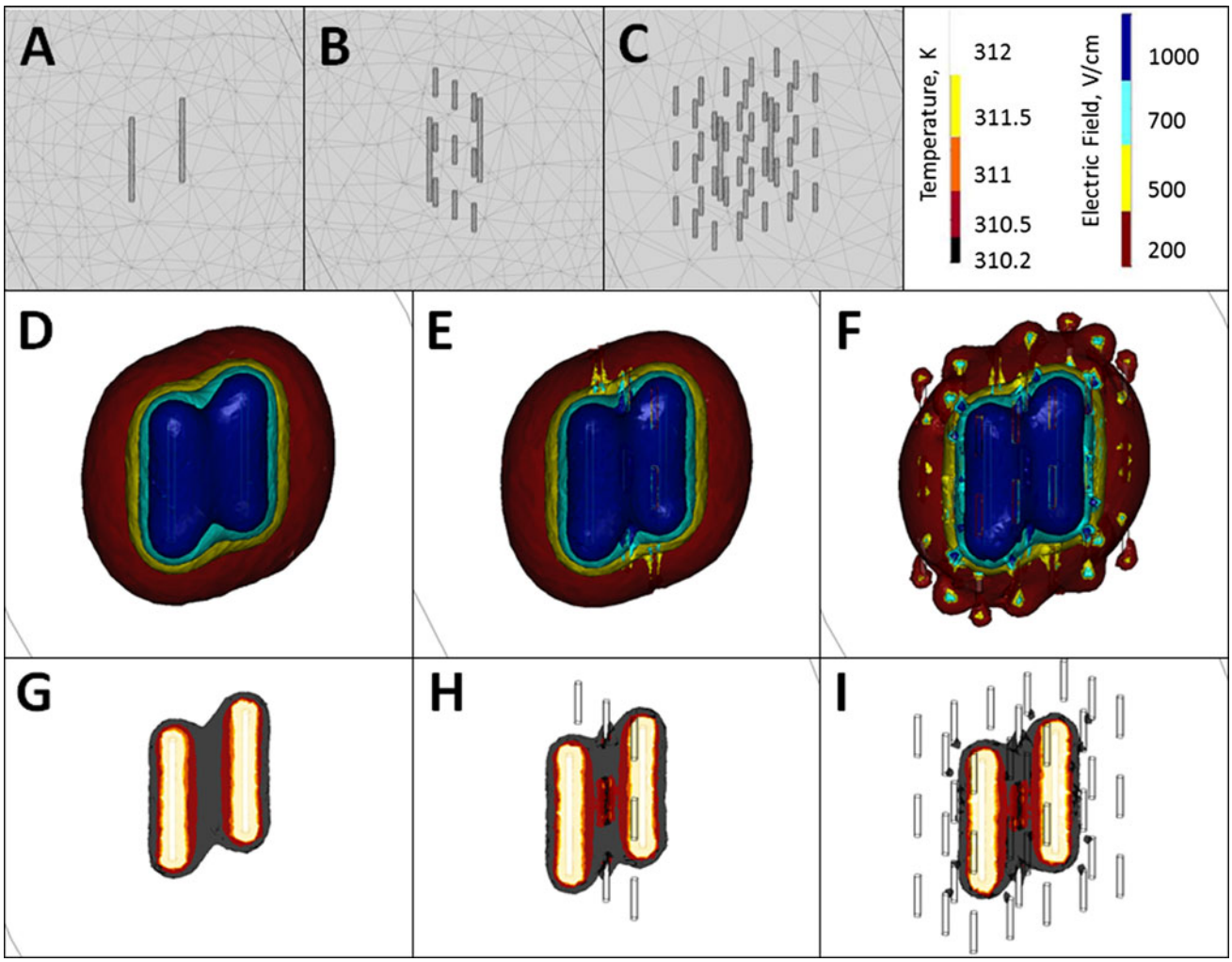

Fig. 5 Electric field and temperature distributions. **A–C** Model physical geometry grid layouts as well as (**D–F**) electric field and (**G–I**) temperature distributions for (**A**, **D**, and **G**) no seeds, (**B**, **E**, and **H**) experimental seed layout, and (**C**, **F**, and **I**) extrapolated seed layout. These results show no significant change in shape or overall distribution of changes to temperature or electric field

Table 3 Numerical model effect of seeds on electrical current and electric field

Electrical current (A)[a]	No seeds	9-Seed array	39-Seed array
Electric field volume exposure (cm^3)[a]	11.2	9.95 (11.0)	9.54 (14.7)
200 V/cm	11.1	10.7 (3.6)	10.5 (5.4)
500 V/cm	3.58	3.50 (2.2)	3.49 (2.5)
700 V/cm	2.19	2.15 (1.8)	2.21 (0.9)
1000 V/cm	1.18	1.14 (3.6)	1.15 (2.5)

[a] Values for seed grids are given as value (percent difference relative to no seeds)

Table 4 Numerical model effect of seeds on temperature

Temperature increase (K) Volume of exposure (cm^3)[a]	No seeds	9-Seed array	39-Seed array
0.2	1.25	1.20 (3.3)	1.22 (0.9)
0.5	0.422	0.416 (1.4)	0.415 (0.3)
1	0.189	0.184 (2.6)	0.198 (8.0)
2	0.0959	0.101 (5.7)	0.108 (6.7)

[a] Values for seed grids are given as value (percent difference relative to no seeds)

electroporation for local recurrence after prostate brachytherapy, where high-conductivity expired radiotherapy seeds remain in or adjacent to the targeted region. Vegetal, numerical, ex vivo, and in vivo models evaluated the macroscopic effect from the metallic seeds on electrical current, electric field, and temperatures in tissue, as well as acute histological effects. There was no significant impact from the presence of seeds on the characteristics influencing electroporation-based therapy outcomes. This study suggests that there should be minimal difference in tissue

response when EBTs are performed in proximity to small metallic materials relative to the tissue alone.

Acknowledgments This work is supported by the Flack Trustees, NSF CAREER Award CBET-1055913, and the Whitaker International Program. The authors thank Anatoly Dritschilo for advising experimental analysis as well as Victoria Earl and the radiology staff of The Alfred Hospital for assistance.

Conflict of interest R. E. Neal and R. V. Davalos hold pending patents and are recipients of royalty payments from Angiodynamics, Inc., for unrelated IRE work. R. V. Davalos received consultancy and research grants from Angiodynamics, Inc., for unrelated IRE work. H. Kavnoudias and K.R. Thomson received donated research materials for unrelated IRE work. R. L. Smith, F. Rosenfeldt, R. Ou, C. A. Mclean have no conflicts of interest to declare.

References

1. Al-Sakere B, Andre F, Bernat C et al (2007) Tumor ablation with irreversible electroporation. PLoS One 2(11):e1135
2. Appelbaum L, Ben-David E, Sosna J, Nissenbaum Y, Goldberg SN (2012) US findings after irreversible electroporation ablation: radiologic-pathologic correlation. Radiology 262(1):117–125
3. Ball C, Thomson KR, Kavnoudias H (2010) Irreversible electroporation: a new challenge in "out of operating theater" anesthesia. Anesth Analg 110(5):1305–1309
4. Boukaram C, Hannoun-Levi J-M (2010) Management of prostate cancer recurrence after definitive radiation therapy. Cancer Treat Rev 36(2):91–100
5. Carrara N (2007) Dielectric properties of body tissues. Italian National Research Council, Institute for Applied Physics, Florence
6. Davalos R, Mir L, Rubinsky B (2005) Tissue ablation with irreversible electroporation. Ann Biomed Eng 33(2):223–231
7. Edd JF, Horowitz L, Davalos RV, Mir LM, Rubinsky B (2006) In vivo results of a new focal tissue ablation technique: irreversible electroporation. IEEE Trans Biomed Eng 53(5):1409–1415
8. Finley D, Belldegrun A (2011) Salvage cryotherapy for radiation-recurrent prostate cancer: outcomes and complications. Curr Urol Rep 12(3):209–215
9. Foster KR, Schwan HP (1989) Dielectric properties of tissues and biological materials: a critical review. Crit Rev Biomed Eng 17(1):25–104
10. Gabriel S, Lau RW, Gabriel C (1996) The dielectric properties of biological tissues: II. Measurements in the frequency range 10 Hz to 20 GHz. Phys Med Biol 41(11):2251–2269
11. Garcia PA, Pancotto T, Rossmeisl JH Jr et al (2011) Non-thermal irreversible electroporation (N-TIRE) and adjuvant fractionated radiotherapeutic multimodal therapy for intracranial malignant glioma in a canine patient. Technol Cancer Res Treat 10(1): 73–83
12. Garcia PA, Rossmeisl JH Jr, Neal RE 2nd, Ellis TL, Davalos RV (2011) A parametric study delineating irreversible electroporation from thermal damage based on a minimally invasive intracranial procedure. Biomed Eng Online 10(1):34
13. Hjouj M, Rubinsky B (2010) Magnetic resonance imaging characteristics of nonthermal irreversible electroporation in vegetable tissue. J Membr Biol 236(1):137–146
14. Ivorra A, Mir LM, Rubinsky B (2009) Electric field redistribution due to conductivity changes during tissue electroporation: experiments with a simple vegetal model. Springer, Berlin, pp 59–62
15. Ivorra A, Rubinsky B (2007) In vivo electrical impedance measurements during and after electroporation of rat liver. Bioelectrochemistry 70(2):287–295 Epub 2006 Oct 2021
16. Kimura M, Mouraviev V, Tsivian M, Mayes JM, Satoh T, Polascik TJ (2010) Current salvage methods for recurrent prostate cancer after failure of primary radiotherapy. BJU Int 105(2): 191–201
17. Miklavcic D, Semrov D, Mekid H, Mir LM (2000) A validated model of in vivo electric field distribution in tissues for electrochemotherapy and for DNA electrotransfer for gene therapy. Biochim Biophys Acta 1523(1):73–83
18. Mir LM, Orlowski S, Belehradek JJ, Teissie J, Rols MP (1995) Biomedical applications of electric pulses with special emphasis on antitumor electrochemotherapy. Bioelectrochem Bioenerg 38:203–207
19. Narayanan G, Froud T, Lo K, Barbery KJ, Perez-Rojas E, Yrizarry J (2012) Pain analysis in patients with hepatocellular carcinoma: irreversible electroporation versus radiofrequency ablation-initial observations. Cardiovasc Intervent Radiol 30:30
20. Neal RE 2nd, Davalos RV (2009) The feasibility of irreversible electroporation for the treatment of breast cancer and other heterogeneous systems. Ann Biomed Eng 37(12):2615–2625
21. Neal RE 2nd, Garcia PA, Robertson JL, Davalos RV (2012) Experimental characterization and numerical modeling of tissue electrical conductivity during pulsed electric fields for irreversible electroporation treatment planning. IEEE Trans Biomed Eng 59(4):1076–1085 Epub 2012 Jan 1076
22. Neal RE 2nd, Rossmeisl JH Jr, Garcia PA, Lanz OI, Henao-Guerrero N, Davalos RV (2011) Successful treatment of a large soft tissue sarcoma with irreversible electroporation. J Clin Oncol 29(13):e372–e377
23. Neal RE 2nd, Singh R, Hatcher HC, Kock ND, Torti SV, Davalos RV (2010) Treatment of breast cancer through the application of irreversible electroporation using a novel minimally invasive single needle electrode. Breast Cancer Res Treat 123(1):295–301
24. Neumann E, Schaefer-Ridder M, Wang Y, Hofschneider PH (1982) Gene transfer into mouse lyoma cells by electroporation in high electric fields. EMBO J 1(7):841–845
25. Onik G, Mikus P, Rubinsky B (2007) Irreversible electroporation: implications for prostate ablation. Technol Cancer Res Treat 6(4):295–300
26. Potters L, Morgenstern C, Calugaru E et al (2008) 12-year outcomes following permanent prostate brachytherapy in patients with clinically localized prostate cancer. J Urol 179(5):S20–S24
27. Rabin Y, Stahovich TF (2003) Cryoheater as a means of cryosurgery control. Phys Med Biol 48(5):619–632
28. Neal RE II, Cheung W, Kavnoudias H, Thomson KR (2012) Spectrum of imaging and characteristics for liver tumors treated with irreversible electroporation. J Biomed Sci Eng 5(12A): 813–818
29. Thomson KR, Cheung W, Ellis SJ et al (2011) Investigation of the safety of irreversible electroporation in humans. J Vasc Interv Radiol 22(5):611–621